Available online at www.sciencedirect.com

SciVerse ScienceDirect

Ceramics International 39 (2013) 1863–1870

CERAMICS INTERNATIONAL

www.elsevier.com/locate/ceramint

Optimization and thermal cycling behavior of $La_2Ce_2O_7$ thermal barrier coatings

Hongying Dong[a], Dongxing Wang[b], Yanling Pei[c], Houyang Li[b], Peng Li[b], Wen Ma[b,*]

[a]School of Chemical Engineering, Inner Mongolia University of Technology, Hohhot 010051, China
[b]School of Materials Science and Engineering, Inner Mongolia University of Technology, Hohhot 010051, China
[c]School of Materials Science and Engineering, Beijing University of Aeronautics and Astronautics, No. 37 Xueyuan Road, Beijing 100191, China

Received 16 June 2012; received in revised form 10 August 2012; accepted 10 August 2012
Available online 17 August 2012

Abstract

The $La_2Ce_2O_7$ (LC) coating with the La/Ce ratio close to 1 was obtained by atmospheric plasma spraying, using $La_2Ce_{2.5}O_8$ as a feedstock powder and optimized spray parameters. The spray distance plays a significant role in terms of phase composition, phase stability, as well as porosity of the LC coating, while keeping other spray parameters constant. The plasma-sprayed coatings were prepared and thermally cycled by gas-burner tests to evaluate thermal cycling lifetime. The thermal cycling lifetime of the LC/YSZ double-layer coating was more than three times the lifetime of a single-layer LC coating and comparable to the YSZ coating at operating temperature of ~1230 °C. The thermal cycling lifetimes of the LC/YSZ coating were ~40% longer at operating temperature of ~1320 °C, but much lower at operating temperature of ~1350 °C compared to the optimized YSZ coating. The failure mechanisms for the LC and LC/YSZ coatings thermally cycled under different conditions were also established in this work.

Keywords: $La_2Ce_2O_7$ (LC); Thermal barrier coatings (TBCs); Thermal cycling; Failure mechanism

1. Introduction

Thermal barrier coatings (TBCs) are widely used to protect and insulate hot-section metal components in gas turbines [1]. Ceramic TBCs are considered technologically important because of their ability to increase the operating temperatures and reduce the cooling requirements for turbine engines, thus achieving higher engine efficiency, lowering emissions and increasing performance of these engineering materials parts [2].

The state-of-the-art topcoat material, which is being used for TBC applications, is yttria partially stabilized zirconia (YSZ) [3,4]. YSZ performs well up to ~1200 °C, but it cannot be long-term used above 1200 °C because of sintering and phase transformations, which lead to the reduction of strain tolerance in combination with an increase of the Young's modulus and a volume change during cooling [5,6]. As a consequence, a considerable reduction of thermal cycling lifetime is observed for current YSZ coating materials when used above 1200 °C. Recently, some new ceramic materials, such as $LaMgAl_{11}O_{19}$, $LaTi_2Al_9O_{19}$, metal–glass composite, ZrO_2–Y_2O_3–La_2O_3, 7.5 mass% Y_2O_3–HfO_2 (7.5 YSH) oxides, $La_2Zr_2O_7$ (LZ), $La_2Ce_2O_7$ (LC), $SrZrO_3$ and other rare earth oxides doped zirconia, have been evaluated as potential TBC materials to further increase the operation temperature of turbine engines [7–16].

$La_2Ce_2O_7$ (LC) is a solid solution of La_2O_3 in CeO_2 with a defect fluorite structure. The main advantages of LC used as a TBC material are due to its low thermal conductivity and no phase transformation between room temperature and 1400 °C [14]. However, the thermal expansion of LC shows a sudden decrease in the temperature range of 200–400 °C caused by the stronger transverse motion compared to the strength of vibration in the crystals; moreover, LC reacts with Al_2O_3 at high temperatures, both of the reasons result in short thermal cycling lifetime of the single-layer LC TBC [14,17]. It seems that the double-layered topcoat design can overcome the

*Corresponding author. Tel./fax: +86 471 657 5752.
E-mail address: wma@imut.edu.cn (W. Ma).

0272-8842/$ - see front matter © 2012 Elsevier Ltd and Techna Group S.r.l. All rights reserved.
http://dx.doi.org/10.1016/j.ceramint.2012.08.034

shortcomings and increase the thermal cycling lifetime of the LZ and LC coatings [18–20]. In most cases, the new TBC candidate materials have low thermal conductivity and high phase stability, but relatively low toughness values compared to YSZ. The double-layered topcoat design makes coating possible to be used at higher temperatures, as well as having longer thermal cycling lifetime than a single-layer YSZ coating.

The objective of the present work is to produce the optimized LC coating both in composition and structure design, i.e. single-layer LC coating or double-layer LC/YSZ coating, which could be used at higher temperatures than possible with the YSZ coating. The thermal cycling performance and the failure mechanism of the LC and the LC/YSZ coatings under the different cycling conditions are investigated.

2. Experimental procedure

Lanthanum–cerium-oxide powder was synthesized by a solid-state reaction using La_2O_3 and CeO_2 (Aldrich, 99.99%). The starting materials were ball-milled and, after drying, sintered at 1400 °C for 24 h and ball-milled again. The single phase lanthanum–cerium-oxide powder was synthesized by repeating the process twice.

For plasma spraying, the synthesized lanthanum–cerium-oxide powder was milled with ethanol and subsequently spray-dried with 1.8 wt% dispersing agent. Sieved size fractions between 45 and 100 μm were used for plasma spraying. The spray dried powder with a nominal composition of $La_2Ce_{2.5}O_8$ as a feedstock powder was used to produce the coatings. Since the coating composition is close to stoichiometric $La_2Ce_2O_7$ by using $La_2Ce_{2.5}O_8$ as a feedstock powder, the coating is named also as LC. The detailed information about the powder composition optimization can be found in our previous work [21]. The YSZ powder used was a 7.8 wt% yttria-stabilized zirconia powder (Metco 204 NS, Sulzer Metco GmbH, Germany).

For thermal cycling, the LC and LC/YSZ (LC on the top) coatings were air plasma sprayed (Triplex I gun, Sulzer Metco, Switzerland) on IN738 substrates which had a diameter of 30 mm and a thickness of 3 mm. The spray parameters for the coatings were argon and helium plasma gas flow rates of 23 and 12 standard liter per minute (slpm), a plasma current of 300 A at a power of 20 kW, and spray distances (SD) of 80–100 mm. The disk-shaped samples had a beveled edge to minimize the effect of stresses originating at the free edges of the samples. Before deposition of the final topcoat, the substrates were coated with a 150 μm Ni–Co–Cr–Al–Y bondcoat by vacuum plasma spraying (VPS) in a Sulzer Metco facility using a F4 gun. Steel substrates were also coated during fabrication of the thermal cycling specimens. These coatings were used to characterize the as-sprayed condition. The freestanding coatings, which were produced by removing the steel substrate from the coating with hydrochloric acid, were used to investigate sintering effect (sample configuration: 10 mm × 25 mm × 600 μm) by applying a high-temperature dilatometer (Netzsch 402E apparatus, Germany), as well as pore-size distribution using mercury porosimeters (Pascal 140 and 440, CE instruments, Italy).

Table 1
Results of thermal cycling tests of the LC and LC/YSZ coatings.

Sample	TBC system	$T_{surface}$ (°C)	$T_{substrate}$ (°C)	Cycles to failure	TGO thickness (μm)
coating-A	LC	1231	970	821	4.8/6.8/5.4
coating-B		1223	973	2574	–/9.2/4.8
coating-C	LC/YSZ	1326	1007	1404	5.4/8.0/5.2
coating-D		1355	1039	77	2.4/4.0/2.8
–	YSZ [22]	1320–1350	1000–1035	250–1000	–

For comparison, the test results of a typical YSZ coating are also given. The thickness of the TGO is measured at three locations on the sample: upper left region, middle region, and lower right region from the images shown in Figs. 6–9.

Thermal cycling was performed on the disk-shaped samples in a gas-burner test facility that was operated under natural gas and oxygen. The details about thermal cycling can be found in our previous work [15]. The results of thermal cycling tests of the LC and LC/YSZ coatings are listed in Table 1.

The microstructures of the coatings were investigated by a scanning electron microscope (SEM) (Model JXA 840, JEOL, Japan). The compositions of the LC freestanding coatings were analyzed by an Inductively Coupled Plasma Optical Emission Spectrometer (ICP-OES) (IRIS Intrepid II XSP, Thermo Fisher, USA). X-ray photoelectron spectroscopy (XPS) (PHI XPS 5600, Physical Electronics, USA) with monochromatic $Al_{K\alpha}$ was used to determine the oxidation state of cerium in the coatings. Gaussian–Lorentzian peaks were fitted to the Ce 3d spectrum after subtraction of a Shirley background.

3. Results and discussion

3.1. Optimization of the LC coating

$La_2Ce_2O_7$ is a solid solution of La_2O_3 in CeO_2 with a fluorite type structure [23], its XRD pattern is similar to that of CeO_2 with a small change of the lattice parameter (CeO_2, $a=5.4113$ Å; $La_2Ce_2O_7$, $a=5.5718$ Å). LC has high phase stability not only from room temperature to 1400 °C but also at 1400 °C for a long period [17]. Due to the difference in vapor pressures between CeO_2 (2×10^{-2} atm, 2500 °C) and La_2O_3 (8×10^{-5} atm, 2500 °C) [24], there is less CeO_2 content in the LC coatings compared with the LC powder. The higher vapor pressure of CeO_2 results in more loss during plasma spraying compared with that of La_2O_3. The LC coating with the La/Ce ratio near to 1 has high phase stability and comparatively long thermal cycling lifetime [21]. The La/Ce ratio increases with increasing the La/Ce ratio in feedstock powder used for air plasma spraying under the same spray parameters. The desired composition of the ceramic topcoat can be adjusted

either by changing the feedstock powder composition or/and by modifying the spray parameters. According to the previous work [21], the feedstock powder with a nominal composition of $La_2Ce_{2.5}O_8$ was chosen to obtain more stoichiometric LC coating. Based on the $La_2Ce_{2.5}O_8$ feedstock powder, the La/Ce ratio change in the coatings was investigated by applying different spray distances, while keeping other spray parameters constant.

The La/Ce ratio in the as-sprayed coatings as a function of the spray distance is shown in Fig. 1. The La/Ce ratio increases with increasing the spray distance from 80 to 100 mm, with the ratios slightly lower than 1 and higher than 1 at the spray distances of 80 mm and 90 mm, respectively.

The DTA curves of the as-sprayed LC coatings at different spray distances are shown in Fig. 2. There is neither endothermic peak nor exothermic peak observed during DTA measurements that were done in the temperature range of 200–1400 °C with the spray distances at 80 mm and 90 mm, suggesting good phase stability. However, a small exothermic peak for the LC coating at the spray distance of 100 mm appears at ~1050 °C, which is attributed to the decomposition of the LC coating. The free energies of surface segregation ($-\Delta G_{seg}$) of lanthanum from its solid solutions in ceria ($La_xCe_{1-x}O_{2-x/2}$) is strongly composition-dependent, decreasing as the lanthanum content is increased and asymptotically approaching a constant value [25]. The $-\Delta G_{seg}$ reaches the minimum value of 6.6 Kcal/mol as the La/Ce ratio equals to 1 in $La_xCe_{1-x}O_{2-x/2}$, whereas the $-\Delta G_{seg}$ increases for the La/Ce ratios that are deviated from 1 to a certain extent. The minimum value of $-\Delta G_{seg}$ implies that lanthanum is more difficult to segregate from $La_2Ce_2O_7$, with a consequence of high phase stability.

In addition to the composition optimization of the coatings, homogeneity of the microstructure was also optimized. The porosity distribution of the LC coatings plasma sprayed at the different spray distances is shown in Fig. 3. The results reveal a typical bimodal pore size distribution. The larger defects corresponding to radii above 1 μm are believed to have resulted from macrocracks and voids. The fine pores smaller than 1 μm are mainly attributed to microcracks such as intersplat gaps and intrasplat cracks. The cumulative porosities of the LC freestanding coatings are ~11.2%, ~10.3% and ~11.5% at the spray distances of 80 mm, 90 mm and 100 mm, respectively. The porosity values of the LC coatings are lower than the optimized porosity level (~15%) normally used in the conventional YSZ-based coatings [26].

Fig. 4 shows the sintering shrinkage kinetics of the LC freestanding coatings plasma sprayed at the spray distances of 80 mm and 90 mm. During the measurements, the LC free-standing coatings were heated from room temperature to 1250 °C (stage 1: heating) with a heating rate of 3 °C/min, and then kept at this temperature

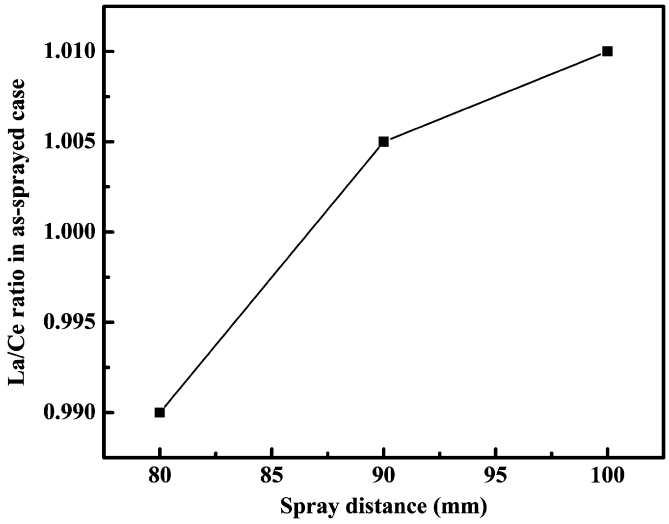

Fig. 1. La/Ce ratio in the as-sprayed coatings versus spray distance.

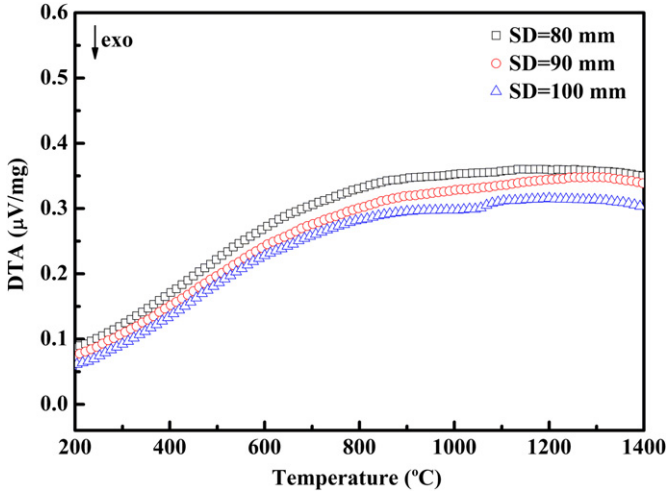

Fig. 2. DTA curves of the as-sprayed LC coatings at the different spray distances.

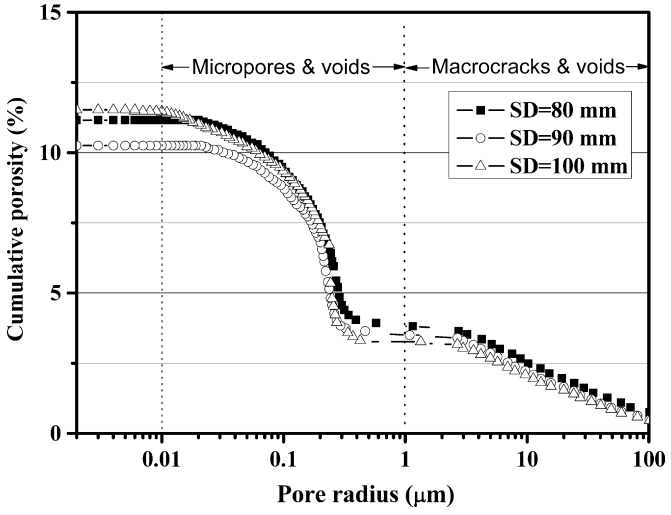

Fig. 3. Porosity distribution of the LC freestanding coatings plasma sprayed at the different spray distances in the as-sprayed case.

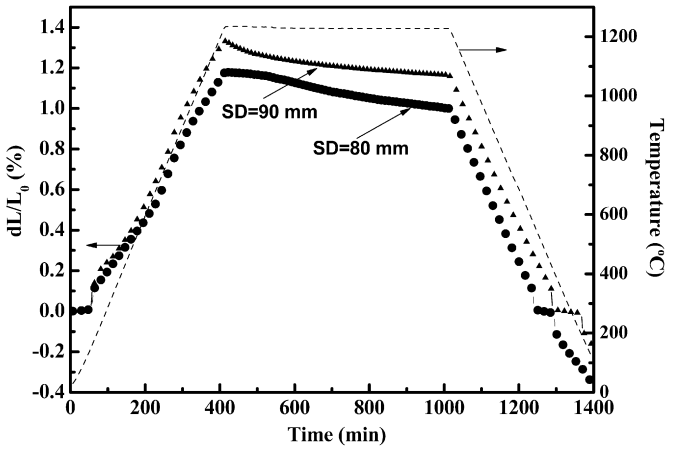

Fig. 4. Sintering shrinkage kinetics of the LC freestanding coatings plasma sprayed at the spray distances of 80 mm and 90 mm.

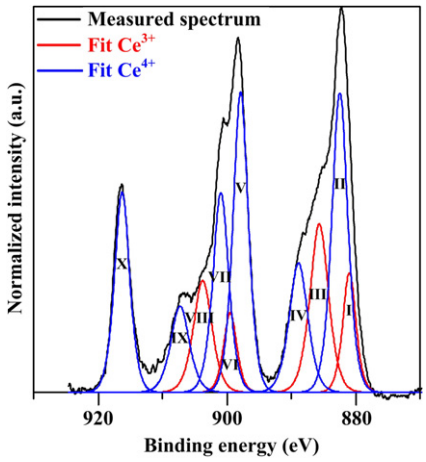

Fig. 5. XPS spectrum of Ce 3d from the LC coating plasma sprayed at the spray distance of 80 mm.

(stage 2: isothermal) for 10 h followed by cooling to room temperature (stage 3: cooling) at a rate of 3 °C/min. The sintering rate of the ceramic TBCs at isothermal stage (stage 2) changes with time, especially in the early sintering period. As shown in Fig. 4, the sintering shrinkage rates (defined as an apparent linear shrinkage rate of a sample during the first 10 h at 1250 °C) of the LC freestanding coatings are calculated as $5.00\times10^{-9}\ s^{-1}$ and $4.67\times10^{-9}\ s^{-1}$ at the spray distances of 80 mm and 90 mm, respectively. The lower sintering shrinkage rate of the LC freestanding coating at the spray distance of 90 mm is attributed to its lower porosity. The curves for both the LC coatings have a sudden change in low temperature range, which is possible due to the crystal lattice contraction. This is also confirmed by Cao et al. [14] in their study of the bulk LC material.

Based on the coating composition and microstructure optimization in terms of spray distance, phase stability, porosity and sintering shrinkage kinetic, the LC coatings plasma sprayed at the spray distance of 80 mm were chosen to evaluate their thermal cycling behavior while keeping other spray parameters constant.

3.2. Thermal cycling behavior of the LC/YSZ coatings

The XPS analysis of the as-sprayed LC coating (SD=80 mm) surface reveals the presence of both Ce^{3+} and Ce^{4+} valence states as shown in Fig. 5. The peaks marked I, III, VI and VIII (881.0, 885.7, 899.5 and 903.9 eV respectively) represent Ce^{3+} while peaks from II, IV, V, VII, IX and X (882.5, 888.9, 897.9, 901.0, 907.3 and 916.3 eV respectively) are from Ce^{4+} ions. Peak marked X is a satellite peak indicating the presence of +4 valence in the as-sprayed coating. The results are in good agreement with Viswanathan's work [27], which is based on a solution precursor plasma sprayed nanoceria coating. The ratio of the integrated area of the curves belonging to Ce^{3+} to that of curves belonging to Ce^{4+} is used to calculate the ratio of Ce^{3+}/Ce^{4+} in the sample, which gives a value of ~0.4 in this case. The diffraction peaks of the LC coatings in the as-sprayed case or after cycling are shifted in lower diffraction angles compared with that of the LC feedstock powder [28], a phenomenon that is believed to be caused by the decomposition of the LC coating during plasma spraying, as well as the partial reduction of Ce^{4+} to Ce^{3+} at elevated temperatures with the larger size of Ce^{3+} (1.143 Å) in comparison with Ce^{4+} (0.97 Å) [29]. The larger size of Ce^{3+} can give an improvement in thermal expansion for the LC coating.

The cycling test results of LC and LC/YSC coatings at different temperatures are listed in Table 1. The data for a typical YSZ coating is also presented for comparison. It is obvious that the coating-A has a short thermal cycling lifetime compared with the YSZ coating. However, the thermal cycling lifetime of the coating-B at a surface temperature of 1223 °C is 2574 cycles, which is comparable to that of the YSZ coating and shows much longer thermal cycling lifetime than that of the coating-A. It indicates that the LC/YSZ coating can really increase the coating lifetime under the same cycling conditions. This was also fairly confirmed by studies in other groups in the $SrZrO_3$/YSZ [15], $LaTi_2Al_9O_{19}$/YSZ [30], $La_2Zr_2O_7$/YSZ [19], and $LaMgAl_{11}O_{19}$/YSZ coatings [31]. The thermal cycles obviously decrease for the coating-C (1404 cycles) and the coating-D (77 cycles) with increasing cycling temperatures. At a surface temperature of ~1320 °C, the thermal cycling lifetime of the coating-C is 1404 cycles, which is ~40% longer, whereas the thermal cycling lifetime of the coating-D at a surface temperature of ~1350 °C is much shorter than that of the YSZ coating.

The cross-section micrograph of the LC coating (coating-A) as-sprayed, surface morphology of the coating-A and its cross-section micrographs after cycling at a surface temperature of 1231 °C are shown in Fig. 6. The as-sprayed coating-A has a homogeneous microstructure with some large pores as shown in Fig. 6(a), which are caused by improper melting of the large particles during

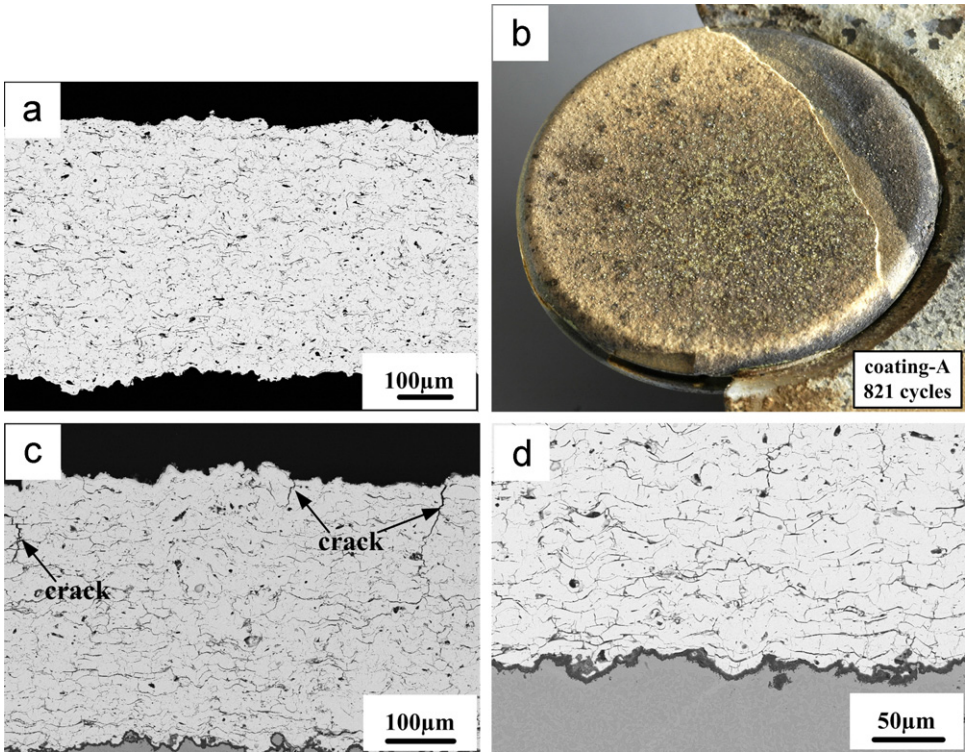

Fig. 6. Cross-section micrograph of the LC coating (coating-A) as-sprayed (a), surface morphology of the coating-A (b) and its cross-section micrographs (c) and (d) after cycling at a surface temperature of 1231 °C.

spraying. The coating-A spalled from the bondcoat (Fig. 6b), whereas the coating-A itself was still intact with a few vertical cracks as shown in Fig. 6(c). It is also intact near topcoat–bondcoat interface even with a TGO average thickness of 6.8 μm (central part), implying that the TGO growth is not the main failure mechanism for the coating-A. The main failure mechanism in this case is the difference in TECs between the topcoat and the bondcoat, especially in low temperature range the TEC of the bulk LC material has a sudden decrease ($3\times10^{-6}\,K^{-1}$, 280 °C)[17]. The TEC sudden decrease of the LC free-standing coating in low temperature range is also evident in Fig. 4. For the LC single-layer coating, the shorter thermal cycling lifetime could be also attributed to the chemical reaction of the LC layer and the underlying TGO mainly consisting of Al_2O_3. It is evident that the chemical reaction degrades the interface bonding between the LC layer and the TGO layer and leads to spallation of TBC [20].

The surface morphology of the LC/YSZ coating (coating-B) and its cross-section micrographs after cycling at a surface temperature of 1223 °C are shown in Fig. 7. The coating-B spalled from the bondcoat (Fig. 7a) and some vertical cracks and horizontal cracks appeared in the LC layer, whereas only some horizontal cracks displayed in the TGO layer and the YSZ layer near to the TGO as shown in Fig. 7(b) and (c). In addition, the interface between the LC layer and the YSZ layer is still intact. The appearance of the vertical cracks and horizontal cracks in the LC layer indicates that a sintering happens with time cumulating. However, there is no chipping spallation observed on the coating surface, indicating that the sintering of the LC layer is not the main failure mechanism for the coating-B. The TGO growth seems to be the important factor determining the coating lifetime in the case, with an average TGO thickness of 9.2 μm (central part). The main failure mechanism for the coating-B is the same as a typical failure mechanism for the YSZ coating, in which the coalition of small cracks and detached areas, which are usually formed due to the defects in the TGO or near the TGO [32,33].

The surface morphology of the LC/YSZ coating (coating-C) and its cross-section micrographs after cycling at a surface temperature of 1326 °C are shown in Fig. 8. The coating-C spalled from the bondcoat and chipping spallation of the LC layer is also observed in Fig. 8(a). Some vertical cracks and large horizontal cracks appeared in the LC layer, whereas only some horizontal cracks displayed in the TGO layer and the YSZ layer near to the TGO as shown in Fig. 8(b) and (c). The interface between the LC layer and the YSZ layer is intact as shown in Fig. 8(d). The failure mechanism for the coating-C is not the same as that of the coating-A, as well as that of the coating-B. It is a combination of both the TGO growth (8.0 μm at central part) and the sintering of the LC layer. The sintering becomes more obviously for the LC coating at a surface temperature of 1326 °C, because the LC coating starts to sinter at ~1280 °C [14,28].

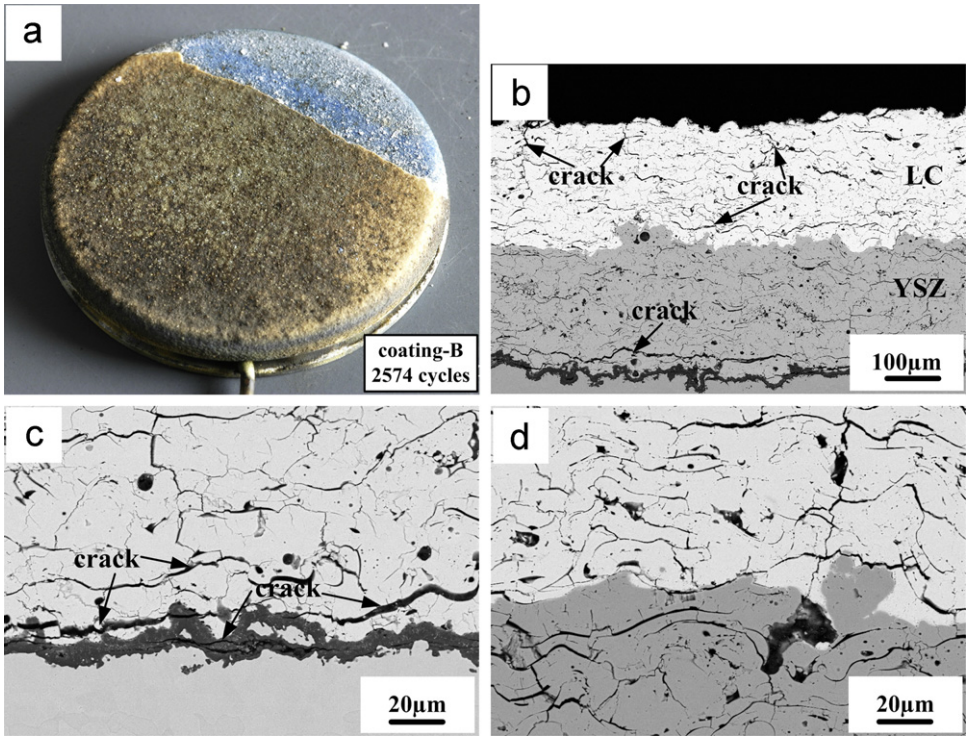

Fig. 7. Surface morphology of the LC/YSZ coating (coating-B) (a) and its cross-section micrographs (b), (c) and (d) after cycling at a surface temperature of 1223 °C.

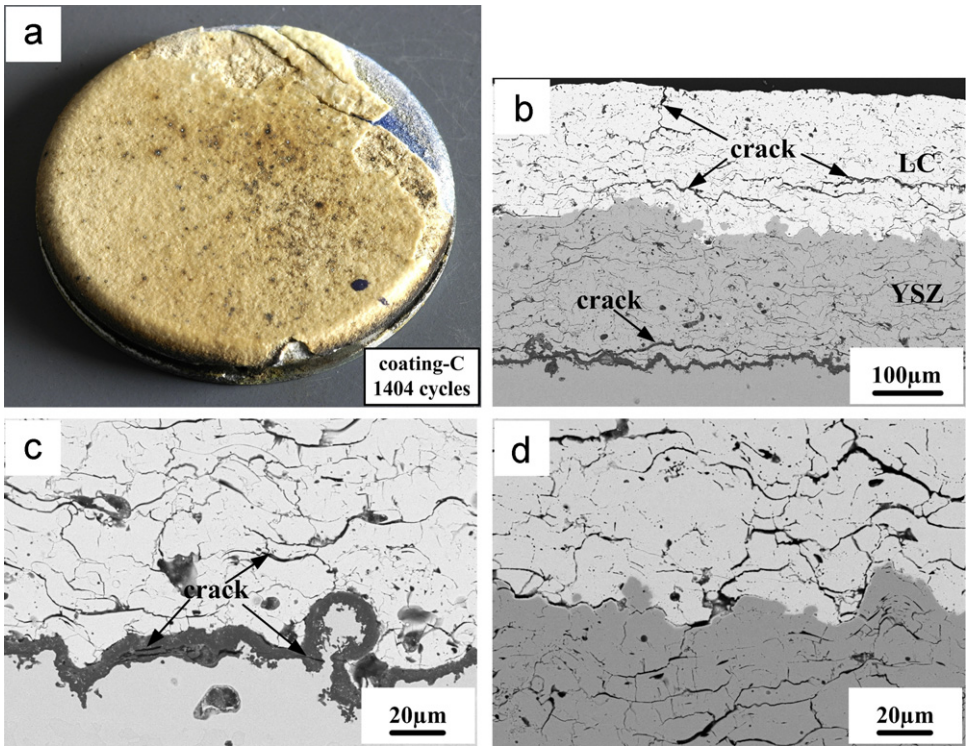

Fig. 8. Surface morphology of the LC/YSZ coating (coating-C) (a) and its cross-section micrographs (b), (c) and (d) after cycling at a surface temperature of 1326 °C.

The surface morphology of the LC/YSZ coating (coating-D) and its cross-section micrographs after cycling at a surface temperature of 1355 °C are shown in Fig. 9. It is evident that only the chipping spallation occurred for the coating-D as shown in Fig. 9(a). A lot of horizontal cracks appeared in the LC coating (Fig. 9b), whereas no horizontal

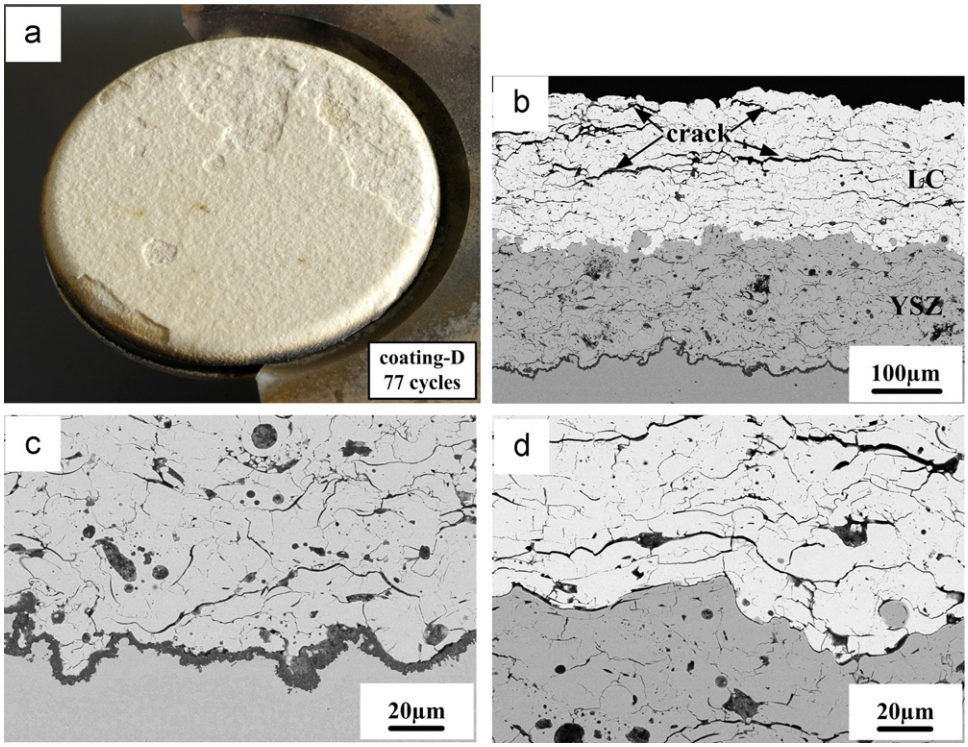

Fig. 9. Surface morphology of the LC/YSZ coating (coating-D) (a) and its cross-section micrographs (b), (c) and (d) after cycling at a surface temperature of 1355 °C.

cracks displayed either in the TGO layer or in the YSZ layer (Fig. 9b and c). The interface between the LC layer and the YSZ layer is also intact as shown in Fig. 9(d). The failure mechanism for the coating-D is only due to the sintering of the LC layer, not because of the TGO growth (4.0 μm at central part). The sintering shrinks the LC layer and introduces in-plane tensile stress that can cause cracks perpendicular to the interface. The in-plane tensile stress is developed in the outer layer due to the restriction of the inner layer in the LC coating during thermal cycling. The horizontal cracks in the outer layers in the LC coating are developed when the in-plane tensile stress accumulates to some extent, which results in the spallation of the outer layers in the LC coating.

4. Conclusions

The atmospheric plasma sprayed LC coating was optimized in terms of chemical composition, phase stability and microstructure by using $La_2Ce_{2.5}O_8$ as a feedstock powder and adjusting the spray distance at 80 mm while keeping other spray parameters constant. The thermal cycling lifetime of the LC/YSZ coating was more than three times the lifetime of a single-layer LC coating and comparable to the lifetime of the YSZ coating at operating temperature of ~1230 °C. A major advantage of the LC/YSZ coating is that its thermal cycling lifetime was ~40% longer than that of the optimized YSZ coating at operating temperature of ~1320 °C, indicating that LC is a superior material for TBC applications at higher temperatures, compared to the current YSZ coating. The difference in TECs, especially in low temperature range, between the LC and the bondcoat is suggested to be the main failure mechanism for the LC coating, whereas the TGO growth is a main failure mechanism for the LC/YSZ coating at operating temperature of ~1230 °C. The combination of the sintering of the LC coating and the TGO growth, and the sintering of the LC coating alone are the main failure mechanisms for the LC/YSZ coating at operating temperatures of ~1320 °C and ~1350 °C, respectively.

Acknowledgments

The authors gratefully acknowledge the financial support by the National Natural Science Foundation of China (51062012 and 51062013), the Key Project of Chinese Ministry of Education (210035) and the Program for New Century Excellent Talents in University (NCET-11–1017). Experiments about thermal cycling tests were finished in Forschungszentrum Jülich GmbH with the help of Prof. R. Vaβen.

References

[1] N.P. Padture, M. Gell, E.H. Jordan, Thermal barrier coatings for gas-turbine engine applications, Science 296 (4) (2002) 280–284.
[2] D. Zhu, R.A. Miller, Thermal conductivity and sintering behavior of advanced thermal barrier coatings, in: H. Lin, M. Singh (Eds.), Ceramic Engineering and Science, in: Proceedings of the 26th Annual

Conference on Composites, Advanced Ceramics, Materials, and Structures: B, vol. 23 (4), John Wiley & Sons, Inc., Hoboken, NJ, USA 2008, pp. 457–468.
[3] W. Nelson, R. Orenstein, TBC experience in land-based gas turbines, Journal of Thermal Spray Technology 6 (2) (1997) 176–180.
[4] J. Wigren, L. Pejryd, Thermal barrier coatings—why, how, where and where to, in: C. Coddet (Ed.), Thermal Spray—Meeting the Challenges of the 21st Century, in: Proceedings of the 15th International Thermal Spray Conference, May, Nice, France, 1998, pp. 1531–1542.
[5] D. Basu, C. Funke, R.W. Steinbrech, Effect of heat treatment on elastic properties of separated thermal barrier coatings, Journal of Materials Research 14 (12) (1999) 4643–4650.
[6] J. Thornton, A. Majumdar, Ceria precipitation and phase stability in zirconia based thermal barrier coatings, in: A. Ohmori (Ed.), Thermal Spraying—Current Status and Future Trends, in: Proceedings of the 14th International Thermal Spray Conference, 22–26 May, Kobe, Japan, 1995, pp. 1075–1080.
[7] R. Gadow, M. Lischka, Lanthanum hexaaluminate – novel thermal barrier coatings for gasturbine applications – materials and process development, Surface and Coatings Technology 151–152 (2002) 392–399.
[8] X. Xie, H. Guo, S. Gong, H. Xu, Lanthanum–titanium–aluminum oxide: a novel thermal barrier coating material for applications at 1300 °C, Journal of the European Ceramic Society 31 (9) (2011) 1677–1683.
[9] M. Dietrich, V. Verlotski, R. Vaßen, D. Stöver, Metal-glass based composites for novel TBC-systems, Material Wissenschaft und Werkstoff Technik 32 (8) (2001) 669–672.
[10] K. Matsumoto, Y. Itoh, T. Kameda, EB-PVD process and thermal properties of hafnia-based thermal barrier coating, Science and Technology of Advanced Materials 4 (2) (2003) 153–158.
[11] M. Matsumoto, N. Yamaguchi, H. Matsubara, Low thermal conductivity and high temperature stability of ZrO_2–Y_2O_3–La_2O_3 coatings produced by electron beam PVD, Scripta Materialia 50 (6) (2004) 867–871.
[12] R. Vaßen, X. Cao, F. Tietz, D. Basu, D. Stöver, Zirconates as a new materials for thermal barrier coatings, Journal of the American Ceramic Society 83 (8) (2000) 2023–2028.
[13] B. Saruhan, P. Francois, K. Fritscher, U. Schulz, EB-PVD processing of pyrochlore-structured $La_2Zr_2O_7$-based TBCs, Surface and Coatings Technology 182 (2–3) (2004) 175–183.
[14] X. Cao, R. Vaßen, W. Fischer, F. Tietz, W. Jungen, D. Stöver, Lanthanum–cerium oxide as a thermal barrier-coating material for high temperature applications, Advanced Materials 15 (17) (2003) 1438–1442.
[15] W. Ma, D.E. Mack, R. Vaßen, D. Stöver, Perovskite-type strontium zirconate as a new material for thermal barrier coatings, Journal of the American Ceramic Society 91 (8) (2008) 2630–2635.
[16] D.R. Clarke, Materials selection guidelines for low thermal conductivity thermal barrier coatings, Surface and Coatings Technology 163–164 (2003) 67–74.
[17] W. Ma, S. Gong, H. Xu, X. Cao, On improving the phase stability and thermal expansion coefficients of lanthanum cerium oxide solid solutions, Scripta Materialia 54 (8) (2006) 1505–1508.
[18] X. Cao, R. Vaßen, F. Tietz, D. Stöver, New double-ceramic-layer thermal barrier coatings based on zirconia—rare earth composite oxides, Journal of the European Ceramic Society 26 (3) (2006) 247–251.
[19] R. Vaßen, D. Stöver, New thermal barrier coatings based on pyrochlore/YSZ double layer systems, International Journal of Applied Ceramic Technology 1 (4) (2005) 351–361.
[20] W. Ma, S. Gong, H. Li, H. Xu, Novel thermal barrier coatings based on $La_2Ce_2O_7$/8YSZ double-ceramic-layer systems deposited by electron beam physical vapor deposition, Surface and Coatings Technology 202 (12) (2008) 2704–2708.
[21] W. Ma, Y. Ma, S. Gong, H. Xu, X. Cao, Thermal cycling behavior of lanthanum-cerium oxide thermal barrier coatings prepared by air plasma spraying, Key Engineering Materials 336–338 (2007) 1759–1761.
[22] F. Traeger, M. Ahrens, R. Vaßen, D. Stöver, A life time model for ceramic thermal barrier coatings, Materials Science and Engineering A 358 (1–2) (2003) 255–265.
[23] F. Brisse, O. Knop, Pyrochlores. II. An investigation of $La_2Ce_2O_7$ by neutron diffraction, Canadian Journal of Chemistry 45 (6) (1967) 609–614.
[24] U. Schulz, B. Saruhan, K. Fritscher, C. Leyens, Review on advanced EB-PVD ceramic topcoats for TBC applications, International Journal of Applied Ceramic Technology 1 (4) (2004) 302–315.
[25] M.F. Wilkes, P. Hayden, A.K. Bhattacharya, Surface segregation of lanthanum and cerium ions in ceria/lanthana solid solutions: comparison between experimental results and a statistical-mechanical model, Applied Surface Science 206 (1–4) (2003) 12–19.
[26] S. Stecura, Optimization of the Ni–Cr–Al–Y/ZrO_2–Y_2O_3 thermal barrier system, Advanced Ceramic Materials 1 (1) (1986) 68–76.
[27] V. Viswanathan, R. Filmalter, S. Patil, S. Deshpande, S. Seal, High-temperature oxidation behavior of solution precursor plasma sprayed nanoceria coating on martensitic steels, Journal of the American Ceramic Society 90 (3) (2007) 870–877.
[28] W. Ma, H. Dong, H. Guo, S. Gong, X. Zheng, Thermal cycling behavior of $La_2Ce_2O_7$/8YSZ double-ceramic-layer thermal barrier coatings prepared by atmospheric plasma spraying, Surface and Coatings Technology 204 (21–22) (2010) 3366–3370.
[29] R.D. Shannon, Revised effective ionic radii and systematic studies of interatomic distances in halides and chalcogenides, Acta Crystallographica A32 (1976) 751–767.
[30] X. Xie, H. Guo, S. Gong, H. Xu, Thermal cycling behavior and failure mechanism of $LaTi_2Al_9O_{19}$/YSZ thermal barrier coatings exposed to gas flame, Surface and Coatings Technology 205 (17–18) (2011) 4291–4298.
[31] X. Chen, Y. Zhao, X. Fan, Y. Liu, B. Zou, Y. Wang, H. Ma, X. Cao, Thermal cycling failure of new $LaMgAl_{11}O_{19}$/YSZ double ceramic top coat thermal barrier coating systems, Surface and Coatings Technology 205 (10) (2011) 3293–3300.
[32] A.G. Evans, J.W. Hutchinson, Y. Wei, Interface adhesion: effects of plasticity and segregation, Acta Materialia 47 (15–16) (1999) 4093–4113.
[33] A. Rabiei, A.G Evans, Failure mechanisms associated with the thermally grown oxide in plasma-sprayed thermal barrier coatings, Acta Materialia 48 (15) (2000) 3963–3976.